

# Multi-center, multi-vendor automated segmentation of left ventricular anatomy in contrast-enhanced MRI

Carla Sendra-Balcells<sup>a</sup>, Víctor M. Campello<sup>a</sup>, Carlos Martín-Isla<sup>a</sup>, David Vilades Medel<sup>b</sup>, Martín Luís Descalzo<sup>b</sup>, Andrea Guala<sup>c</sup>, José F. Rodríguez Palomares<sup>c</sup>, Karim Lekadir<sup>a</sup>

<sup>a</sup>*Dept. de Matemàtiques i Informàtica, Universitat de Barcelona*

<sup>b</sup>*Unitat d'Imatge Cardíaca, Hospital de Sant Creu i Sant Pau*

<sup>c</sup>*Cardiovascular Imaging Unit, Aortic diseases and Inherited cardiomyopathies (CSUR), Hospital Universitari Vall d'Hebron*

---

## Abstract

**Background:** Accurate delineation of the left ventricular boundaries in late gadolinium-enhanced magnetic resonance imaging (LGE-MRI) is an essential step for scar tissue quantification and patient-specific assessment of myocardial infarction. Many deep-learning techniques have been proposed to perform automatic segmentations of the left ventricle (LV) in LGE-MRI showing segmentations as accurate as those obtained by expert cardiologists. Thus far, the existing models have been overwhelmingly developed and evaluated with LGE-MRI datasets from single clinical centers with homogeneous imaging protocols and characteristics. However, in practice, LGE-MRI images vary significantly between clinical centers within and across countries, in particular due to differences in the MRI scanners, imaging conditions, contrast injection protocols and local clinical practise.

**Methods:** This work investigates for the first time multi-center and multi-vendor LV segmentation in LGE-MRI, by proposing, implementing and evaluating in detail several strategies to enhance model generalizability across clinical sites. These include data augmentation to artificially augment the image variability in the training sample, image harmonization to align the distributions of LGE-MRI images across clinical sites, and transfer learning to adjust existing single-center models to unseen images from new clinical sites.

**Results:** The results obtained based on a new multi-center LGE-MRI dataset acquired in four clinical centers in Spain, France and China, show that the combination of data augmentation and transfer learning can lead to single-center models that generalize well to new clinical centers not included in the original training.

**Conclusions:** The proposed framework shows the potential for developing clinical tools for automated LV segmentation in LGE-MRI that can be deployed in multiple clinical centers across distinct geographical locations.

*Keywords:* Late gadolinium-enhanced magnetic resonance imaging (LGE-MRI), Multi-center image segmentation, Generalizable deep learning

---

\*Corresponding author

Email address: [carla.sendra@ub.edu](mailto:carla.sendra@ub.edu) (Carla Sendra-Balcells)

## 1. Background

### 1.1. Problem and motivation

Patient-specific assessment of myocardial infarction (MI), one of the leading causes of morbidity and mortality worldwide [1], is routinely performed in clinical practice based on late gadolinium-enhanced magnetic resonance imaging (LGE-MRI). The image modality enables to highlight the presence and extent of scar tissues in the left ventricular myocardium. A prerequisite for scar tissue quantification is the accurate delineation of the boundaries of the left ventricle (LV) [2]. While LV automated segmentation on cine-MRI has been extensively investigated [3], application of existing solutions to LGE-MRI is faced with additional challenges due to the intensity heterogeneity arising from the accumulation of contrast agent in the infarcted myocardium. This introduces artefacts within and outside of the myocardium, which affect the definition of the endo- and epi-cardial boundaries. Furthermore, the number, location, shape and size of the scar tissues can vary greatly across patients, which further complicates the development of robust LV segmentation methods in LGE-MRI. As a result, while many research and commercial tools are already in use for cine-MRI, LV segmentation in LGE-MRI still relies on labor-intensive manual delineation in clinical practice.

To address this problem, researchers investigated three main families of solutions over the last decade. Initially, registration-based approaches were attempted, such that the LV boundaries extracted from the cine-MRI images were propagated onto the LGE-MRI images after non-rigidly aligning the corresponding images ([4], [5], [6]). Such an approach, however, suffered from a lack of robustness due to inherent differences in appearance between the cine- and LGE-MRI images. Later on, deformable models were proposed to better guide the LV segmentation process in LGE-MRI images, by directly encoding the shape and appearance variability of the infarcted myocardium [7]. However, the local heterogeneity induced by the scarred areas and contrast enhancements continued to pose difficulties, affecting the robustness of the existing techniques. Finally, with the advent of deep learning, a new generation of techniques were developed to better encode the complexity found in LGE-MRI images based on convolutional neural networks ([8], [9], [10], [11]). Despite their promise, these techniques have suffered from one important limitation, namely that the neural networks have been almost systematically trained and validated with an LGE-MRI sample from a single clinical center. Because neural networks are known to lack generalizability to unseen domains, these methods have had limited clinical applicability at scale thus far.

The problem in question is often referred to as the domain shift problem, and has been attracting increased attention recently in the medical image analysis community. For example, a recent challenge on this topic was organized in the cardiac MRI domain at the 2020 Medical Image Computing & Computer-Assisted Intervention conference (MICCAI 2020) by the University of Barcelona, in collaboration with six Spanish, German and Canadian clinical centres. Entitled "Multi-Center, Multi-Vendor and Multi-Disease Cardiac Segmentation (M&Ms)", the study demonstrated that single-center, single-vendor neural networks do not generalize naturally when segmenting cine-MRI images with distinct imaging domains [12]. Multi-center LGE-MRI segmentation is even more challenging as, in addition to differences in populations, especially when applying the models across continents and ethnic groups, LGE-MRI samples show even further variability in imaging conditions between cardiology centres, depending on the scanner vendors, imaging sequences, contrast injection protocols and local clinical practice. In particular, the time between contrast injection and LGE-MRI image acquisition can vary greatly between centers, typically between 7 minutes up-to to a total of 10 minutes, resulting in differences in contrast wash-out and image formation. As a result, the LGE-MRI appearance, both globally and locally, can have marked differences as clearly illustrated Figure 1 based on images from four different hospitals. At the same time, the limited numbers of available LGE-MRI datasets compared to cine-MRI images, combined with legal and

organizational obstacle across centers and countries, has made access to interoperable multi-center LGE-MRI datasets more difficult, which has further limited the development of generalizable models for LGE-MRI segmentation.

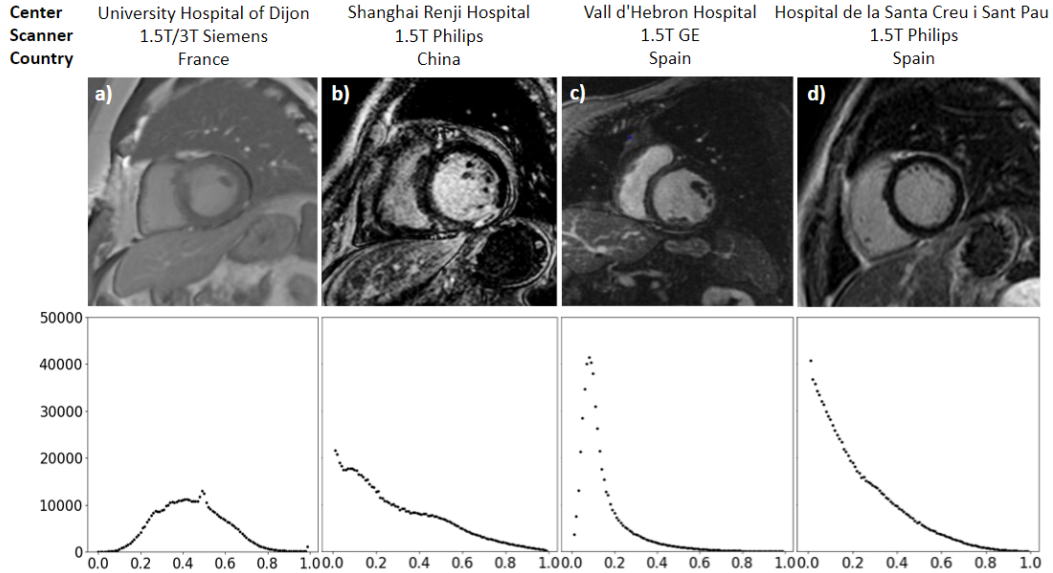


Figure 1: Four LGE-MRI images together with the average intensity distribution of each dataset, acquired in 4 different hospitals. Each histogram has a very different shape and shows the variability between centers in terms of image intensities.

### 1.2. Goals and contributions

This work emerges to address the need for automated segmentation methods in LGE-MRI that can be applied reproducibly across clinical centers, while resolving for inherent biases due to differences in scanner vendors and imaging protocols. To the best of our knowledge, only one work has thus far included a multi-center and multi-vendor LGE-MRI dataset [13], but no generalization technique was studied to enable scalability beyond the training datasets. Instead, in this work, we present the first deep learning pipeline that explores specific mechanisms to achieve generalizability to unseen clinical centers. To this end, several techniques were investigated, optimized and systematically evaluated, including data augmentation, domain mixing, transfer learning and domain adaptation. This work is based on a unique multi-center LGE-MRI dataset acquired with three distinct scanner vendors (Siemens, Philips and General Electric) in four hospitals located in three countries (France, Spain and China). The results show that single-center neural networks enriched with suitable generalization procedures can reach and even surpass the performance of multi-center, multi-vendor models, hence eliminating the need for comprehensive multi-center datasets to train generalizable LGE-MRI models for future cardiac patient assessment.

## 2. Methods

In this work, a very first end-to-end pipeline is investigated for the segmentation of the LV, including its blood pool and myocardium, in multi-center LGE-MRI contexts. To this end, four dif-

ferent approaches are explored to enhance the generalizability across sites of existing neural networks for LGE-MRI segmentation, as schematically represented in Figure 2. These include:

1. Data augmentation techniques to artificially extend the data distribution captured by the trained models.
2. Image harmonization to align the data distributions of the training and testing images.
3. Transfer learning to adjust the neural network to the new clinical center based on very few unseen images.
4. Multi-center models directly trained with data from multiple clinical centers, which are used for comparative evaluation of the different generalization mechanisms.

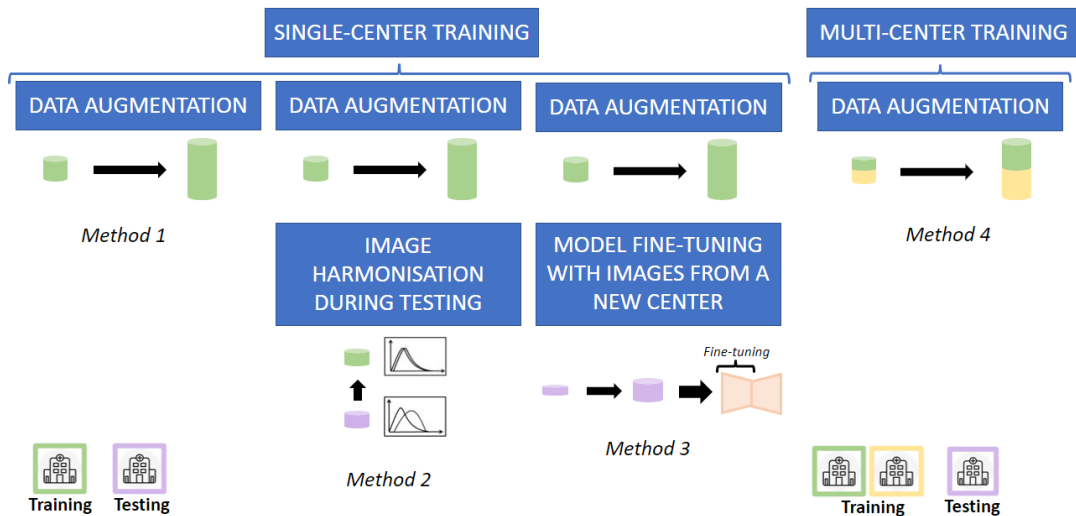


Figure 2: Four different approaches implemented in this work to enhance the generalisability of LGE-MRI segmentation models across distinct clinical sites.

We confirm that all experiments were performed in accordance with relevant guidelines and regulations.

### 2.1. Datasets

The multi-center and multi-vendor dataset used in this study consists of 216 LGE-MRI cases acquired in four different clinical centers as detailed in Table 1. Two out of four samples are publicly available datasets from France and China, while the two other samples correspond to new LGE-MRI images acquired in two different hospitals in Spain. The subjects have been scanned by using a range of scanner vendors by Siemens, Philips or General Electric (GE). In addition to having distinct intensity distributions as observed in Figure 1, the multi-center LGE-MRI images also differ in the image resolution (0.75-1.88 mm), slice thickness (5-13 mm), and acquisition time after contrast injection (7 to 10 minutes). The samples from each clinical site are described in more detail next.

#### 2.1.1. EMIDEC dataset: University Hospital Dijon, France

This dataset was compiled as part of the automatic Evaluation of Myocardial Infarction from Delayed-Enhancement Cardiac MRI challenge (EMIDEC) [14]. The EMIDEC volunteers included 33

Table 1: Details of the multi-centre LGE-MRI datasets and characteristics of the acquired images used in this work. Imaging time = Acquisition time after contrast injection.

Dataset	Clinical centre	Country	MRI scanner	Imaging time (mins)	In-plane resolution (mm)	Slice thickness (mm)	Number of slices	Sample size
EMIDEC	University Hospital of Dijon	France	1.5T and 3T Siemens	10	1.37-1.88	8-13	4-10	100
MSCMR	Shanghai Renji Hospital	China	1.5T Philips	-	0.75	5	10-18	45
VH	Vall d'Hebron Hospital	Spain	1.5T GE	10	1.48-1.68	10	8-15	41
STPAU	Sant Pau Hospital	Spain	1.5T Philips	7-10	1.18	5	18-24	30

healthy and 67 diseased subjects, for a total of 100 studies. The data was acquired at the University Hospital of Dijon, France, using Area 1.5 T as well as Skyra 3T Siemens MRI scanners. Slice thickness and in-plane spatial resolution varied greatly, being comprised between 8 and 13 mm and 1.37 and 1.88 mm, respectively. The manual segmentation of the LV blood pool and myocardium were performed by a cardiologist with over 10 years of experience. It is the largest of the four samples and hence it was used as the reference sample for training the single-center neural networks.

#### 2.1.2. MSCMR dataset: Shanghai Renji Hospital, China

The MSCMR dataset was obtained from the Multi-sequence Cardiac MR Segmentation Challenge and it comprises a total of 45 patients suffering from various cardiomyopathies ([15], [16]). The images were acquired at the Shanghai Renji hospital, China, which will allow us to evaluate generalizability across countries as well as continents in this study. Compared to EMIDEC, the MSCMR dataset has a higher image resolution (in-plane resolution = 0.75 mm, slice thickness = 5 mm for all scans) and all images were acquired with a 1.5 T Philips scanner. The manual delineations were initially performed by trainees and later on validated by expert cardiologists.

#### 2.1.3. VH dataset: Vall d'Hebron Hospital, Spain

The VH dataset consists of 41 LGE-MRI datasets acquired at the Vall d'Hebron University Hospital, located in Barcelona, Spain. In addition to covering a new geographical location, namely Spain, the VH sample has several differences with EMIDEC and MSCMR, including the disease group (MI) and the MRI scanner (1.5 T GE scanner). Manual annotations of the LV boundaries were generated by a trained rater using the cvi42 software. The study was approved by the ethics committee of the Vall d'Hebron Hospital and written informed consent was obtained from all participants.

#### 2.1.4. STPAU dataset: Sant Pau Hospital, Spain

The STPAU dataset comprises 30 LGE-MRI cases acquired at the Sant Pau Hospital in Barcelona, Spain. While the clinical center is located in the same region as for the VH sample, the dataset covers a different disease group (ischemic and non-ischemic cardiomyopathy) and was acquired using an MRI scanner from a different vendor (Philips Achieva 1.5T) and a higher-resolution imaging protocol. Furthermore, the time delay between contrast injection and image acquisition varies between 7 and 10 minutes, which adds extra variability. The manual annotations were also performed using cvi42, as in the previous case. All patients signed the informed consent, the study protocol was approved by the Ethical Committee for Clinical Research of our region, and it follows the ethical guidelines of the Declaration of Helsinki.

## 2.2. Single-center model with data augmentation

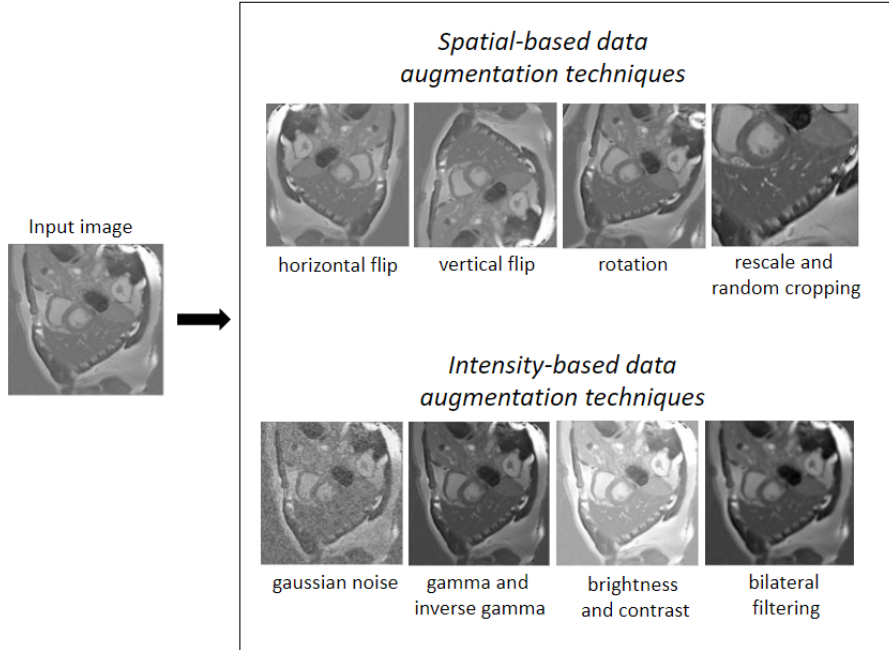


Figure 3: Both spatial and intensity-based data augmentation techniques are applied together with a probability of 0.2 each. From only one slice many samples can be generated, increasing the size of the original dataset significantly.

In this work, we first investigate the potential of data augmentation to enhance the generalizability of LGE-MRI segmentation models (Method 1 in Figure 2). Data augmentation has been widely used to create more robust neural networks by increasing the size as well as the heterogeneity of training samples synthetically. However, the promise of data augmentation is yet to be examined for LGE-MRI, where there is higher complexity due to inherent variability in scar characteristics and contrast appearance.

In this work, we investigate several operators for data augmentation in the context of LGE-MRI as illustrated in Figure 3 and described as follows.

1. **Spatial-based data augmentation:** In addition to the natural variability between cardiac anatomies, especially across countries and ethnic groups, patients undergoing LGE-MRI typically suffer from regional remodelling of the ventricles due to the presence of scar tissue. Hence, spatial-based data augmentation is proposed using the following operators:
  - Horizontal and vertical flips to generate images with different orientations.
  - Random rotations of up to  $\pm 30$  degrees, to simulate different positions of the heart.
  - Random rescaling in the  $[0.75, 1.88]$  mm range so that the model can process images and hearts that vary in size. This range is defined by the minimum and maximum voxel size of our multi-center dataset.
  - Random cropping, such that the training images have the same dimensions of  $256 \times 256$  pixels but with a variation in the position of the heart in the image.

Table 2: Number of subjects for each of the four datasets used during the training, validation and testing phases when data augmentation is implemented in a single-center setting.

Dataset	Training	Validation	Testing
EMIDEC	68	17	15
MSCMR	24	6	15
VH	21	5	15
STPAU	12	3	15

2. **Intensity-based data augmentation:** Because the LGE-MRI appearance can vary between images acquired using different MRI scanners and scanning protocols, such as due to differences in acquisition time after contrast injection, we implemented the following intensity-based data augmentation techniques:

- Bilateral filtering to generate blurred and less detailed copies of the original images.
- Gaussian noise with a standard deviation ranging between  $[0, 0.03]$  to generate artificial noise and image artifacts.
- Gamma and inverse Gamma function with magnitude  $[0.7, 1.5]$  to generate synthetic images with different lighting.
- Brightness and contrast with magnitude  $[-0.5, 0.5]$  to support brightness and contrast variations in the training images.

Each data augmentation technique is applied with a probability of 0.2 during the training of the model. Then, this data augmentation pipeline is evaluated by measuring the final generalization ability of the network (Method 1 in Figure 2). Table 2 summarizes the split of the data used for the training, validation and testing of the model in each experiment.

### 2.3. Image harmonization at testing

While the data augmentation operations focused on improving model generalizability at training, we propose to apply image harmonization at the testing stage to further reduce the discrepancies between the multi-center LGE-MRI images (Method 2 in Figure 2). Image harmonization enables to transform the testing LGE-MRI images from a new clinical center such that their intensity distribution matches as much as possible the imaging characteristics of the single center used to train the baseline neural network. Concretely, two main image harmonization techniques were implemented:

1. **Histogram matching:** It consists of transforming the testing images from the unseen center such that the histogram of the pixel intensity values is superimposed as much as possible with the corresponding histogram extracted from the training images from the training clinical center. The transformation from the testing data (B: target data) to the training data (A: source data) is illustrated in Figure 4(i).
2. **CycleGAN:** Another strategy to address the domain shift between multiple centers is domain adaptation, which can be used to learn the image translation from the source domain to the target domain. To this end, we choose to implement a CycleGAN architecture [17], based on an unpair image-to-image translation. Given that CycleGAN uses cycle consistency, it would learn the translation from the target domain (B) to the source domain (A), and viceversa (Figure 4(ii)). Both target to source and source to target generators are saved in each implementation, decreasing to 6 the number of implementations needed. The amount of samples used to train

Table 3: Number of samples used for the training and validating each CycleGAN model built to harmonise the imaging properties from the different clinical centres.

Dataset		Training		Validation	
Source	Target	Source	Target	Source	Target
EMIDEC	MSCMR	24	24	6	6
EMIDEC	VH	21	21	5	5
EMIDEC	STPAU	12	12	3	3
MSCMR	VH	21	21	5	5
MSCMR	STPAU	12	12	3	3
VH	STPAU	12	12	3	3

each of the CycleGAN models are summarized in Table 3, adjusting for each case the percentage of images from each center so that it is adequately balanced (50% source and 50% target data).

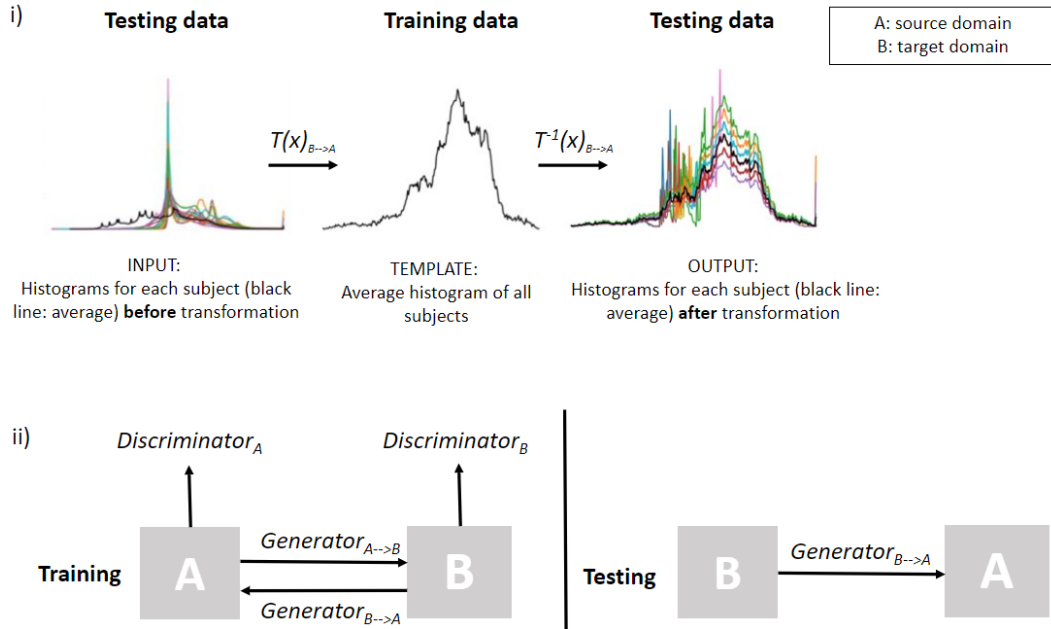


Figure 4: Schematic illustration of the image harmonisation techniques used in this work to make the intensity distributions from the different clinical sites as aligned as possible. First, histogram matching is used to learn a transformation of the histogram of each image from the unseen clinical sites (B) onto the original training clinical centre (A). Second, CycleGAN architecture is used to learn the mapping between the training and the testing clinical center.

#### 2.4. Transfer learning from the original to the new clinical site

Another strategy investigated in this work to improve the scalability of single-center models consisted of applying the so-called transfer learning paradigm, by fine-tuning specific layers of the neural network with a reduced number of LGE-MRI images from the new clinical site (Method 3 in Figure 2). The approach has shown promise for multi-center image segmentation in cardiac



Table 4: List and number of samples used for training and validating multi-centre models in this study.

Dataset	Training	Validation
EMIDEC	42	10
EMIDEC+MSCMR	21+21	5+5
EMIDEC+VH	21+21	5+5
EMIDEC+MSCMR+VH	14+14+14	3+3+3
EMIDEC+MSCMR+VH+STPAU	11+11+11+11	3+3+3+3

cine-MRI [18], but is yet to be demonstrated for multi-center LGE-MRI imaging, where there is increased variability. The following steps are implemented in this work:

1. Initiate the training of the neural network with the EMIDEC dataset, then evaluate the minimum number of fine-tuned layers, in both the decoder and the encoder, that are needed during transfer learning to obtain the maximal segmentation performance on the new LGE-MRI datasets from the remaining clinical centers.
2. Compare the previous results with the segmentations obtained based on a multi-center model directly trained each time with images from two clinical centers (EMIDEC and the new center).
3. Estimate the minimum percentage of images needed from the second clinical center during the fine-tuning to obtain the desired level of performance.
4. Implement the same approach from the previous point but this time by using a model pre-trained on a large dataset (n=350) from cine-MRI (M&M’s dataset), to evaluate transfer learning from a related cardiac MRI modality for which data is abundantly available.

### 2.5. Multi-center model

A fourth and last modelling strategy, i.e. training the neural networks directly from multiple centers (Method 4 in Figure 2), is used for comparative evaluation of the three extended single-center models described in the previous section, i.e. enriched with data augmentation, image harmonization and transfer learning. In this study, we investigated the amount of new centers/domains that are needed to bridge the domain gap in LGE-MRI segmentation, by using a balanced dataset with the same number of subjects for each multi-center data combination, namely EMIDEC, EMIDEC+MSCMR, EMIDEC+VH, EMIDEC+MSCMR+VH and ALL centers. The samples used for training the multi-center models in each combination of datasets/centers are listed in Table 4. In all experiments, the same testing dataset is used for comparative evaluations (n=15).

### 2.6. Baseline workflow

#### 2.6.1. Pre-processing

Min-max normalization is used after cropping of the image to keep the same intensity range in images from the same dataset.

#### 2.6.2. Post-processing

A post-processing is applied to all predictions generated by the model by keeping only the largest connected component of the segmentation volume. This step is commonly used in medical image segmentation, especially in organ imaging, to help on the detection of false positives.

### 2.6.3. Network architecture

As a baseline model, a U-Net architecture is implemented to perform the LV boundary segmentations in LGE-MRI based on some of the modifications proposed by [19] for improved model training as follows. First, Leaky ReLU is used as activation function, then instance normalization is applied after each hidden convolutional layer to stabilise the training. Deep supervision is included to allow gradients to be injected deeper into the network and facilitating the training of all layers. Furthermore, a 2D architecture is selected as it is suitable to address the differences in slice thickness between clinical centers, as well as slice misalignment due to respiratory and cardiac motion artefacts. The encoder and decoder architecture of the model are illustrated in Figure 5.

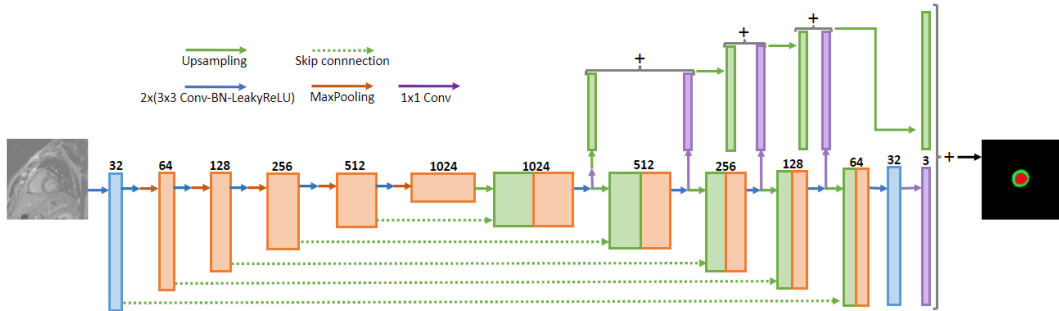


Figure 5: U-Net architecture composed by 6 layers, increasing progressively the number of feature maps until 1024. Additionally, deep supervision layers are included in the decoder.

### 2.6.4. Implementation details

PyTorch is the open-source machine learning library for Python used for the implementation of the model learning. The stochastic gradient descent (SGD) optimization is performed with Adam and the batch size of 16 slices is constrained by the 8 GB of memory of the NVIDIA GeForce RTX 2080 Ti GPU. The learning rate is kept to  $1 \cdot 10^{-3}$  during every training, while the dice and cross entropy losses are calculated at every iteration to optimize the network parameters. The neural network is trained 250 epochs each time and takes half an hour approximately to converge. During testing, each LGE-MRI image segmentation takes less than one second. The main criterion followed to split each dataset in subgroups is 80% for the training and 20% for the validation part, while keeping 15 subjects for the testing.

### 2.6.5. Performance evaluation

For all experiments and results, the performance of each method will be assessed with the average 3D Dice Coefficient (DC), which calculates the overlap ratio between the automatically generated and ground truth segmentations. The measure is estimated by:

$$DC = \frac{2 \cdot (X \cap Y)}{X + Y} = \frac{2 \cdot TP}{2 \cdot TP + FP + FN}, \quad (1)$$

where X and Y are the set of pixels from the automated and true labels of the target structures, while TP, FP, and FN are the corresponding true positives, false positives and false negatives, respectively.

### 3. Results

This section presents detailed experimental results obtained by evaluating and comparing the different strategies proposed for enhancing model generalizability in LGE-MRI segmentation based on single-center models.

#### 3.1. Experiment 1: Effect of data augmentation

In the first experiment, we will evaluate the added value of the different types of data augmentation, including spatial and intensity-based data augmentations. Figure 6 shows the comparative results obtained by three different models: (i) a single-center model without data augmentation (blue line), (ii) a single-center model with spatial data augmentation (orange), and (iii) a single-center model enriched with both spatial and intensity based data augmentations (green). The datasets/centers used for training the single-center model, as well as for testing unseen LGE-MRI images, were permuted to test data augmentation under different scenarios (e.g. sample size). It can be seen from the results that, independently of the clinical center used for training, data augmentation consistently improves the segmentation performance for LGE-MRI, increasing the DC value up to 0.7 units with respect to the baseline model without data augmentation. Furthermore, the results in Figure 6 show that while most of the improvement can be achieved by spatial data augmentation (orange line), intensity-based data augmentation adds value to the approach, in particular when training on the largest sample (EMIDEC) and testing on the smaller samples (MSCMR, VH and STPAU). Having demonstrated the added value of data augmentation, it will be included in all subsequent experiments and results.

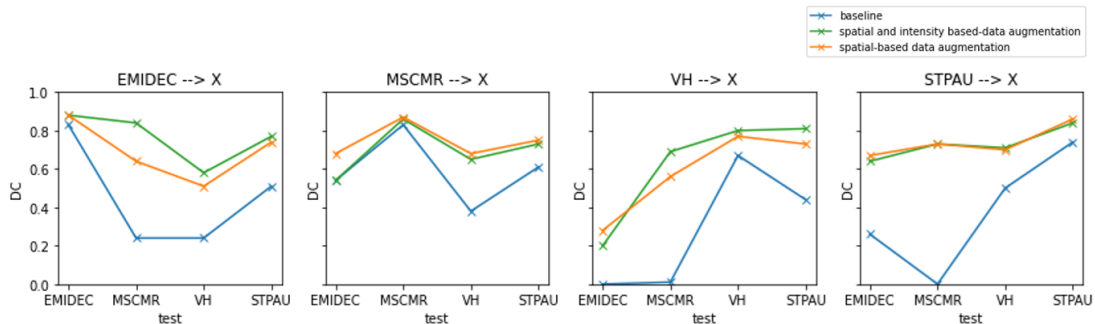


Figure 6: Comparison of single-centre models without and with data augmentation, including spatial and intensity based. X corresponds to each testing dataset not included in the training.

#### 3.2. Experiment 2: Effect of image harmonization

Here, the impact of image harmonization is evaluated when applied to match the testing LGE-MRI images from a new clinical center based on the distribution of the training set from the original site. Specifically, we evaluate three approaches, namely (i) the baseline model with data augmentation from Experiment 1 but without any normalization, (ii) baseline model with histogram matching, and (iii) baseline model with CycleGAN normalization. The results are given in Figure 7, clearly showing that, overall, the two harmonization operations (green and orange lines) do not improve significantly the LGE-MRI segmentations over the baseline model without harmonization (blue line). There are few exceptions, however, such as when the baseline single-center model is trained on the VH sample and tested on the EMIDEC centre using histogram matching.

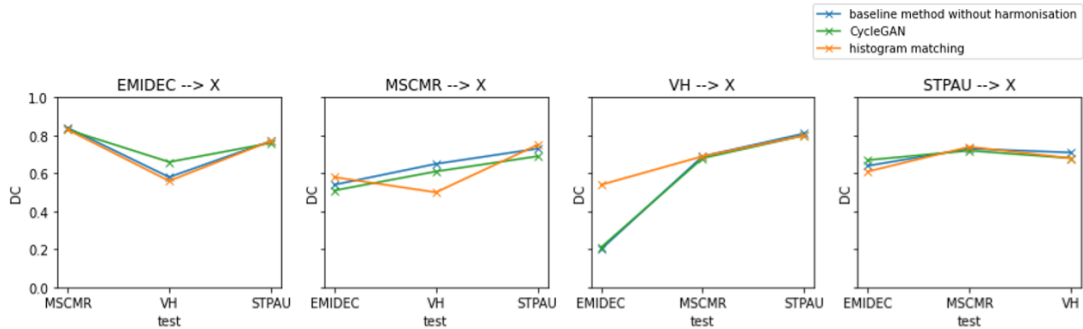


Figure 7: Effect of histogram matching and CycleGAN harmonisation for LGE-MRI segmentation in unseen clinical centres. X corresponds to each testing centre not included in the training dataset.

### 3.3. Experiment 3: Effect of transfer learning

This section evaluates the potential value of transfer learning such that the baseline single-center model is fine-tuned based on a few datasets from the new clinical centers. Figure 8 shows the performance of the transfer learning when the baseline model is trained on EMIDEC as the largest sample and tested on the remaining clinical centers (MSCMR, VH and STPAU). The red and blue lines in the figure show the segmentation accuracy results when the fine-tuning is performed on the encoder and decoder of the neural network, respectively. The black line corresponds to the ideal segmentation model obtained by training the neural network from all LGE-MRI of the new clinical center. It can be seen that the DC values increase with the number of fine-tuned blocks and the maximum is obtained when 5 blocks of the encoder are fine-tuned [20], reaching nearly the same performance as the single-center model of the new center (black line). Furthermore, in Figure 9, the single-center models fine-tuned based on 5 encoding blocks are directly compared to multi-center models trained based on all images from the original and new clinical centers. It can be seen that the fine-tuned models (blue bars) -despite being fine-tuned on the new LGE-MRI images- achieve similar segmentation performances than models directly trained from multi-center image data (green bars). This shows the potential of transfer learning to adjust and optimize a few layers of the existing single-center model based on unseen LGE-MRI images from a new clinical center.

However, transfer learning using model fine-tuning requires manual annotations of some images from the new clinical sites. Hence, ideally the number of new annotated images required to suitably adapt the existing model to the new center should be minimal. In Figure 10, we evaluated the impact of the number of new LGE-MRI images used for fine-tuning. The results indicate that the fine-tuning of single-center models with a small percentage of the target data is sufficient to reach a desirable segmentation accuracy. Such generalisation is achieved, for example, in the case of a single-center model pre-trained with the EMIDEC dataset and fine-tuned using only 10% (about 1-3 subjects) from the new dataset. Finally, Table 5 quantitatively summarizes the capacity of transfer learning to adjust existing models to new centers with minimal effort and sample size.

### 3.4. Experiment 4: Comparison to a multi-center scenario

Finally, in this section, we evaluate the added value of training multi-center models for LGE-MRI segmentation by including training images from multiple clinical sites (i.e. from 1 to 4 centres, considering all samples included in this study). In Figure 11 different combinations of the four datasets processed in this study were explored, either by using a baseline model, data augmentation

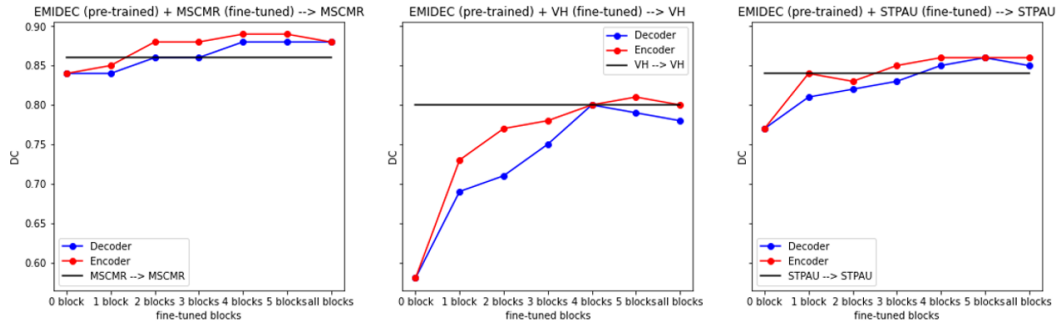


Figure 8: Evaluation of a single-centre model pre-trained on the EMIDEC dataset and fine-tuned with a new clinical dataset (MSCMR, VH or STPAU). Red: Fine-tuning of a number of blocks in the encoder. Blue: Fine-tuning of a number of blocks in the decoder. Black: Model trained from scratch with only the new dataset.

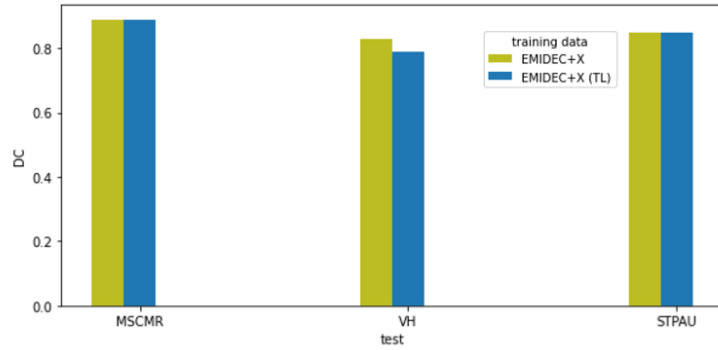


Figure 9: Model trained from scratch using EMIDEC and a second dataset (X), which can be MSCMR, VH or STPAU (green). Then, a model pre-trained with EMIDEC, and fine-tuned and evaluated on X (blue). TL: transfer learning.

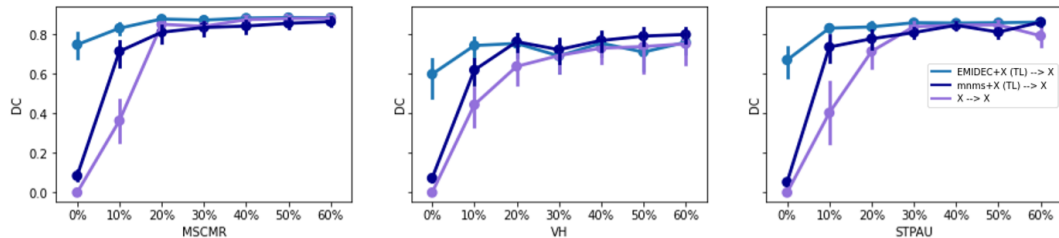


Figure 10: Impact of sample size (percentage) of the new LGE-MRI dataset used for fine-tuning existing single-centre models to a different clinical centre.

or histogram matching. It can be seen that when the model is trained with no data augmentation (baseline), the multi-centre data enhanced the generalisation ability, since the average DC values increase abruptly, while the standard deviation decreases. However, when data augmentation is included in the pipeline, there is no gain for adding new clinical sites to the training stage, as the data augmentation alone is sufficiently powerful for training the model with reduced over-fitting when tested in new centers. The results also confirm that histogram matching does not show significant

Table 5: DC obtained after a) fine-tuning a pre-trained model with the 10% of the data, b) fine-tuning using the 100% of the data, c) training from scratch using the 10% of the data and d) training from scratch using the 100% of the data. The model is pre-trained with the EMIDEC dataset.

Target dataset (X)	a) Fine-tuning with 10% of X (DC)	b) Fine-tuning with 100% of X (DC)	c) Training from scratch with 10% of X (DC)	d) Training from scratch with 100% of X (DC)
MSCMR	<b>0.83</b>	0.89	0.36	0.86
VH	<b>0.74</b>	0.81	0.44	0.80
STPAU	<b>0.83</b>	0.86	0.40	0.84

positive impact on the final performance.

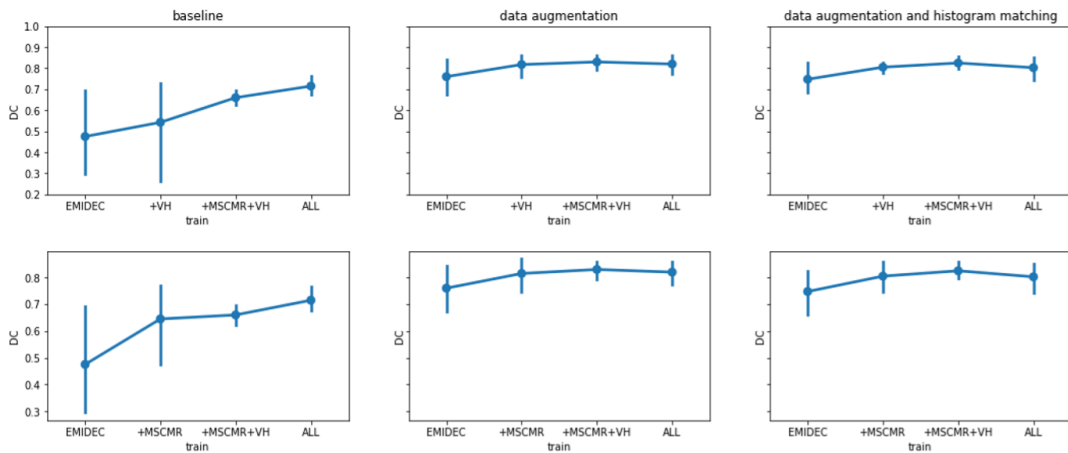


Figure 11: Average DC achieved by models trained on different combinations of clinical datasets, with and without data augmentation, as well as with histogram matching. The first model is initially trained with the EMIDEC dataset, and then new datasets are included progressively from the three other clinical sites.

#### 4. Discussion

In this work several approaches were implemented and tested for delivering generalizable end-to-end pipelines for the segmentation of the left ventricular anatomy in LGE-MRI. This pipeline is built with the purpose to train single-centre models that can maintain a good level of performance when used to segment out-of-sample images from new hospitals. The results highlight the importance of using data augmentation, including both spatial and intensity-based transformations, in particular when there is a high domain shift between the training and unseen clinical site, e.g. EMIDEC in our results. After applying adequate data augmentation to existing single-center models, it was found that neither multi-center training nor image harmonization techniques are needed to obtain additional generalizability, confirming the results obtained by [12] in the M&Ms study for a multi-center and multi-vendor cine-MRI. This finding shows that single-center LGE-MRI models can generalize well if appropriately enriched with data augmentation, which results in an important practical benefit: Multi-center training is difficult in practice as there is a lack of labelling harmonization between centers, in addition to the legal and other obstacles that make difficult cross-site data shar-

ing. Moreover, multi-center models are still specific to those clinical centers that contributed data, whereas there is need for models that can generalize well beyond the training data.

Regarding domain adaptation, which theoretically is a promising solution, existing research has shown that histogram matching could lead to hidden noise in some images after the post-processing [21], while CycleGANs would typically require substantial training data from the new clinical center to achieve a good model performance. In addition to data augmentation, the results demonstrated that transfer learning can positively impact the model performance across sites. This method is based on the fine-tuning of an existing model initially pre-trained on a single-center dataset and adjusted with few datasets from the new clinical site. The obtained results indicate that fine-tuning the first 5 blocks of the encoder of the model with the 10% of the dataset, ranging from 1 to 3 subjects, is sufficient to achieve the desired LV segmentation accuracy in LGE-MRI. For example, a neural network pre-trained based on the EMIDEC dataset and fine-tuned with one subject/image only from STPAU performs as good as a model trained from scratch with the 100% of the STPAU images (Table 5). In terms of computational time, the first model is completely trained in half an hour and the posterior fine-tuning requires only 5 minutes.

In addition to transfer learning focused on LGE-MRI, we evaluated the potential of fine-tuning a pre-existing model trained on larger cine-MRI datasets from the M&M's dataset, which consists of a 350 training images. Despite the different imaging characteristics between cine and LGE-MRI images, in particular the additional presence of scar tissue and contrast enhancements in the LGE-MRI images, the results showed that such cross-modality transfer learning results in enhanced generalizability. This can be easily explained by the fact that such pre-trained multi-center and multi-disease model encodes additional inter-subject variability which aids generalizability also in multi-center and multi-disease LGE-MRI context.

Finally, to illustrate the success of data augmentation and transfer learning to build models with good generalization ability, Figure 12 provides two examples of challenging LGE-MRI cases, with varying imaging and anatomical characteristics. Despite the fact that these images are from two different clinical centers and vary greatly in the appearance, size, shape and location of the scar tissues, the proposed enriched models are capable to accurately identify the LV boundaries consistently across the LGE-MRI examples.

Compared to other multi-center existing studies, such as the M&Ms challenge that comprises 350 cine-MRI cases, the present multi-center LGE-MRI study has a lower sample size. This is because the LGE-MRI datasets are less abundant and more difficult to compile for research studies. Nevertheless, the results in this work are generated based on 216 datasets from four clinical centers, three vendors (Siemens, Philips and GE) and three countries from two different continents.

Another limitation is that this work was focused on the segmentation of the LV anatomy and did not consider the more challenging task of segmenting the scar tissues. This is due to the fact that the clinical annotations for the scar tissues were not available for the two clinical centers in Spain. Future multi-center studies in LGE-MRI should also investigate generalizability of neural networks for scar tissue segmentation. However, our work is an important first step in this direction, and one that will encourage the development of more generalizable models based on data augmentation and transfer learning, in LGE-MRI but also in other cardiac and non-cardiac imaging modalities.

While the proposed framework shows promise for generalizability across multi-center LGE-MRI datasets with challenging and heterogeneous conditions, it can fail to accurately identify the LV boundaries in a few exceptions. As illustrated in Figure 13, a number of failures have been observed in the presence of low-quality images with artifacts due to suboptimal contrast wash-out or highly complex scar appearance. Furthermore as reported in previous works in cardiac cine-MRI segmentation [22], apical and basal slices are also more error-prone than mid-ventricle slices in LGE-MRI segmentation. In fact, even experienced cardiologists can disagree on the segmentation of the LV

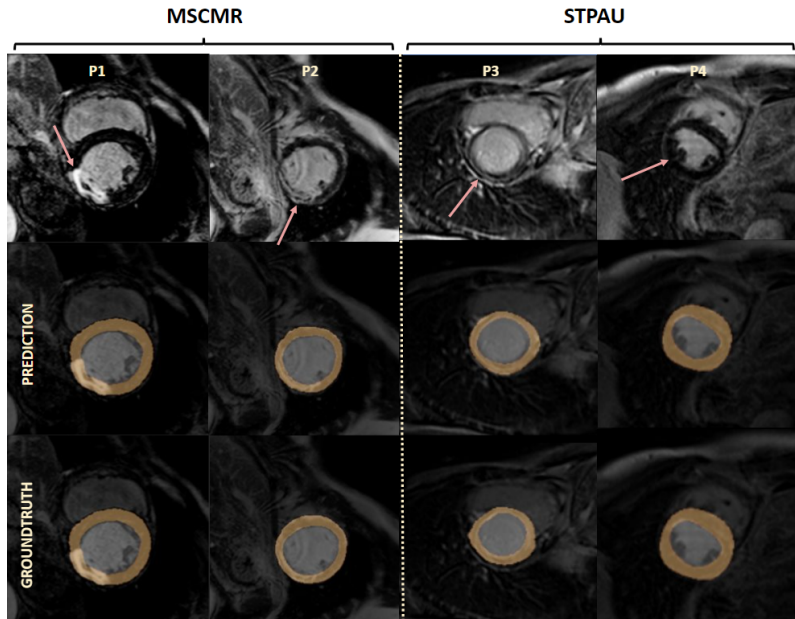


Figure 12: Challenging cases leading to good model predictions on two patients from two different hospitals. First row: original image, second row: prediction, third row: groundtruth. Each of the two columns correspond to images obtained from MSCMR or STPAU datasets respectively. The red arrows highlight the infarct or scar tissue.

borders closer to the apex and base, which generates inter-operator variability that can confuse neural networks, as illustrated in Figure 14.

## 5. Conclusions

This work was motivated by the need for new deep learning based solutions for segmenting the left ventricular anatomy in LGE-MRI in a robust manner across hospitals, scanner vendors, and imaging protocols. Data augmentation extended the image distribution in single-center settings and proved to be an effective technique to generate models with a prominent generalisation ability to new clinical centers. Instead, image harmonization did not improve the capability of single-center models when tested on unseen clinical sites. Furthermore, the exploitation of transfer learning based on fine-tuning of pre-trained models with as little as one additional subject from the new clinical site translated into a substantial improvement of the model's performance.



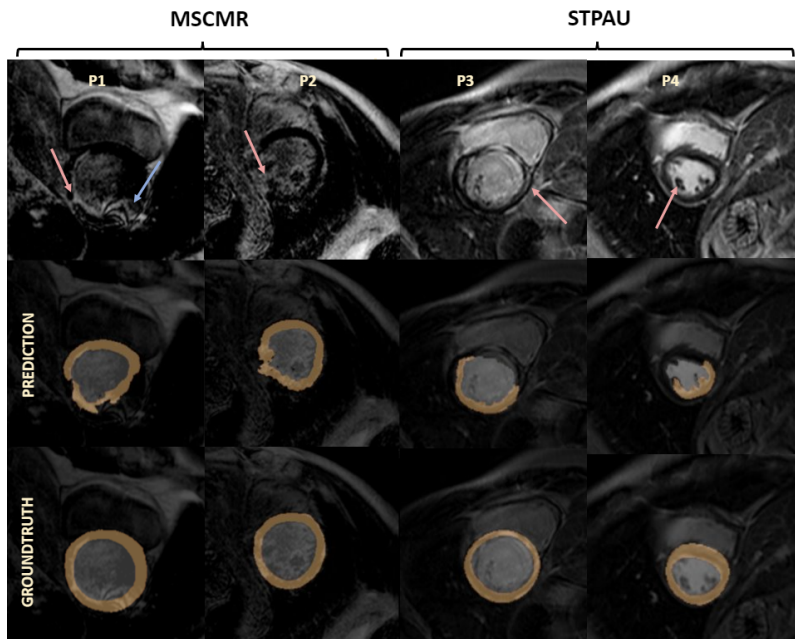


Figure 13: Segmentation failures obtained due to artifacts and highly complex scars. First row: original image, second row: prediction, third row: groundtruth. Each of the two columns correspond to images obtained from MSCMR and STPAU datasets respectively. The blue arrow shows an image artifact, while the red arrows points to the infarct or scar tissue.

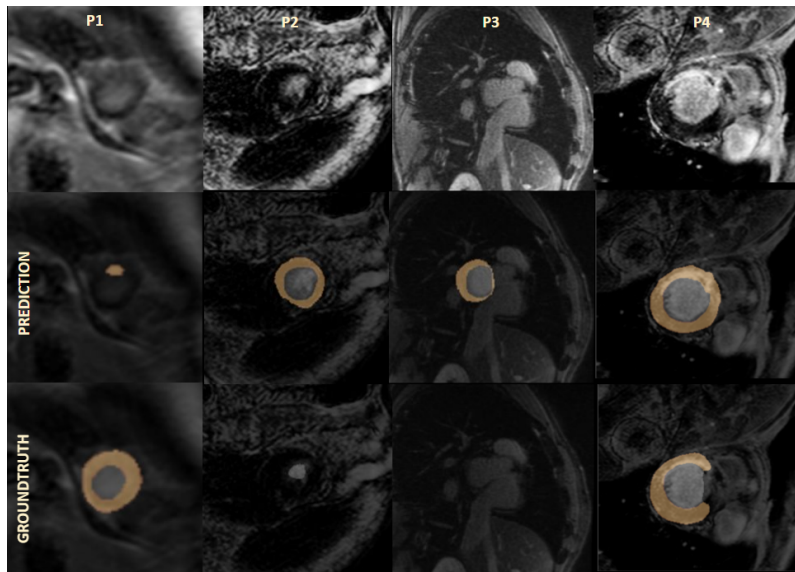


Figure 14: Examples of segmentation failures obtained at the apical and basal slices. First row: original image, second row: prediction, third row: groundtruth. First and second column show two similar cases where both apical slices are segmented differently. The third and fourth columns are two heterogeneous segmentation at the basal region.

## Funding

This work received funding from the European Union’s 2020 research and innovation programme under grant agreement No. 825903 (euCanSHare project), as well as from the Spanish Ministry of Science, Innovation and Universities under grant agreement RTI2018-099898-B-I00. Guala A. received funding from the Spanish Ministry of Science, Innovation and Universities (IJC2018-037349-I).

## Abbreviations

Late gadolinium-enhanced magnetic resonance imaging (LGE-MRI); Left ventricle (LV); Myocardial infarction (MI); Magnetic resonance imaging (MRI); General electric (GE).

## Availability of data and materials

EMIDEC and MSCMR dataset are publicly available. The VH and STPAU datasets are available from the corresponding author upon reasonable request.

## Competing interests

The authors declare that they have no competing interests.

## Authors’ contributions

Design of the work: CSB, VMC, CMI, KL. Image collection: DVM, MLD, AG, JFRP. Interpretation of results: CSB, VMC, CMI, KL. Manuscript draft: CSB, KL. Manuscript review: VMC, CMI, AG, KL.

## References

- [1] H. A. Katus, L. K. Newby, J. Ravkilde, G. A. Beller, R. Bonow, E. E. Van Der Wall, T. B. Ferguson, P. G. Steg, B. F. Uretsky, D. O. Williams, et al., Universal definition of myocardial infarction, *European Heart Journal* 28 (2007) 2525–2538.
- [2] A. Doltra, B. Hoyem Amundsen, R. Gebker, E. Fleck, S. Kelle, Emerging concepts for myocardial late gadolinium enhancement mri, *Current cardiology reviews* 9 (3) (2013) 185–190.
- [3] C. Chen, C. Qin, H. Qiu, G. Tarroni, J. Duan, W. Bai, D. Rueckert, Deep learning for cardiac image segmentation: A review, *Frontiers in Cardiovascular Medicine* 7 (2020) 25.
- [4] D. Wei, Y. Sun, S.-H. Ong, P. Chai, L. L. Teo, A. F. Low, Three-dimensional segmentation of the left ventricle in late gadolinium enhanced mr images of chronic infarction combining long-and short-axis information, *Medical image analysis* 17 (6) (2013) 685–697.
- [5] Q. Tao, S. R. Piers, H. J. Lamb, R. J. van der Geest, Automated left ventricle segmentation in late gadolinium-enhanced mri for objective myocardial scar assessment, *Journal of Magnetic Resonance Imaging* 42 (2) (2015) 390–399.
- [6] C. O. Leong, E. Lim, L. K. Tan, Y. F. Abdul Aziz, G. S. Sridhar, D. Socrates, K. H. Chee, Z.-V. Lee, Y. M. Liew, Segmentation of left ventricle in late gadolinium enhanced mri through 2d-4d registration for infarct localization in 3d patient-specific left ventricular model, *Magnetic resonance in medicine* 81 (2) (2019) 1385–1398.
- [7] J. Liu, X. Zhuang, L. Wu, D. An, J. Xu, T. Peters, L. Gu, Myocardium segmentation from de mri using multicomponent gaussian mixture model and coupled level set, *IEEE Transactions on Biomedical Engineering* 64 (11) (2017) 2650–2661.

- [8] Q. Yue, X. Luo, Q. Ye, L. Xu, X. Zhuang, Cardiac segmentation from lge mri using deep neural network incorporating shape and spatial priors, in: *International Conference on Medical Image Computing and Computer-Assisted Intervention*, Springer, 2019, pp. 559–567.
- [9] F. Zabihollahy, M. Rajchl, J. A. White, E. Ukwatta, Fully automated segmentation of left ventricular scar from 3d late gadolinium enhancement magnetic resonance imaging using a cascaded multi-planar u-net (cmput-net), *Medical physics* 47 (4) (2020) 1645–1655.
- [10] T. Kurzendorfer, K. Breininger, S. Steidl, A. Maier, R. Fahrig, Left ventricle segmentation in lge-mri using multiclass learning, in: *Medical Imaging 2019: Image Processing*, Vol. 10949, International Society for Optics and Photonics, 2019, p. 1094929.
- [11] X. Zhuang, J. Xu, X. Luo, C. Chen, C. Ouyang, D. Rueckert, V. M. Campello, K. Lekadir, S. Vesal, N. RaviKumar, et al., Cardiac segmentation on late gadolinium enhancement mri: a benchmark study from multi-sequence cardiac mr segmentation challenge, *arXiv preprint arXiv:2006.12434*.
- [12] V. M. Campello, P. Gkontra, C. Izquierdo, C. Martín-Isla, A. Sojoudi, P. M. Full, K. Maier-Hein, Y. Zhang, Z. He, J. Ma, et al., Multi-centre, multi-vendor and multi-disease cardiac segmentation: The m&ms challenge, *IEEE Transactions on Medical Imaging*.
- [13] A. S. Fahmy, U. Neisius, R. H. Chan, E. J. Rowin, W. J. Manning, M. S. Maron, R. Nezafat, Three-dimensional deep convolutional neural networks for automated myocardial scar quantification in hypertrophic cardiomyopathy: a multicenter multivendor study, *Radiology* 294 (1) (2020) 52–60.
- [14] A. Lalande, Z. Chen, T. Decourselle, A. Qayyum, T. Pommier, L. Lorgis, E. de la Rosa, A. Cochet, Y. Cottin, D. Ginjac, et al., Emidec: A database usable for the automatic evaluation of myocardial infarction from delayed-enhancement cardiac mri, *Data* 5 (4) (2020) 89.
- [15] X. Zhuang, Multivariate mixture model for cardiac segmentation from multi-sequence mri, in: *International Conference on Medical Image Computing and Computer-Assisted Intervention*, Springer, 2016, pp. 581–588.
- [16] X. Zhuang, Multivariate mixture model for myocardial segmentation combining multi-source images, *IEEE transactions on pattern analysis and machine intelligence* 41 (12) (2018) 2933–2946.
- [17] J.-Y. Zhu, T. Park, P. Isola, A. A. Efros, Unpaired image-to-image translation using cycle-consistent adversarial networks, in: *Proceedings of the IEEE international conference on computer vision*, 2017, pp. 2223–2232.
- [18] C. Ma, Z. Ji, M. Gao, Neural style transfer improves 3d cardiovascular mr image segmentation on inconsistent data, in: *International Conference on Medical Image Computing and Computer-Assisted Intervention*, Springer, 2019, pp. 128–136.
- [19] F. Isensee, P. F. Jaeger, S. A. Kohl, J. Petersen, K. H. Maier-Hein, nnu-net: a self-configuring method for deep learning-based biomedical image segmentation, *Nature Methods* 18 (2) (2021) 203–211.
- [20] M. Amiri, R. Brooks, H. Rivaz, Fine tuning u-net for ultrasound image segmentation: Which layers?, in: *Domain Adaptation and Representation Transfer and Medical Image Learning with Less Labels and Imperfect Data*, Springer, 2019, pp. 235–242.

- [21] P. Garg, T. Jain, A comparative study on histogram equalization and cumulative histogram equalization, *International Journal of New Technology and Research* 3 (9) (2017) 263242.
- [22] C. Chen, W. Bai, R. H. Davies, A. N. Bhuva, C. H. Manisty, J. B. Augusto, J. C. Moon, N. Aung, A. M. Lee, M. M. Sanghvi, et al., Improving the generalizability of convolutional neural network-based segmentation on cmr images, *Frontiers in cardiovascular medicine* 7 (2020) 105.